ROYAL SOCIETY
OF CHEMISTRY

PAPER

Check for updates

Thickness-dependent electronic and optical properties of two-dimensional perovskite oxide films: a first-principles study

Huali Hao,[a] Yuanbin Xue,*[b] Cheng Huang[c] and Xiaojing Bai[b]

The size effect has a significant impact on the properties of thin film materials; however, relevant research in the field of two-dimensional (2D) perovskite films is not yet sufficient. In this study, the size effects on the electronic and optical properties of 2D CdTiO$_3$ (CTO) and SrTiO$_3$ (STO) films were investigated by first-principles calculations. The results demonstrate that the band gaps of both CTO and STO films decrease as the film thickness increases, and CTO films display unique work function characteristics. Further analysis reveals that the electronic effective mass of CTO films decreases significantly with increasing thickness, while the electronic effective mass of STO films remains relatively stable. Moreover, the electron transition probability of CTO films increases markedly when the thickness exceeds 3 unit-cell layers; conversely, STO films exhibit maximum electron transition probability in the monolayer limit. The reasons for these phenomena can be attributed to the differences in the electronic state distribution and orbital characteristics between the two types of films. Our findings provide fundamental insights into the structure−property relationships and offers theoretical guidance for the rational design of 2D perovskite-based electronic devices.

1. Introduction

Thin films with nanometer-scale thicknesses commonly exhibit a size effect, where their physical and chemical properties are strongly dependent on thickness.[1–3] This effect plays a crucial role in determining the functionalities of thin films; for example, thickness variations can significantly influence key material characteristics such as crystallinity and surface morphology, which in turn control performances.[4] In some cases, the film thickness approaches or even falls below certain intrinsic lengths, including electron and phonon mean free paths, exciton Bohr radii, and dislocation spacings, causing the properties of related systems to become dominated by surface, interface, and quantum confinement effects.[5,6]

The size effect has been widely reported across diverse material properties.[7–9] For example, in the mechanical domain, nanocrystalline films can achieve ultrahigh hardness. Electrical and superconducting characteristics of thin films are thickness sensitive.[2,10,11] Studies have shown that the resistivity of CuIn$_{0.8}$Ga$_{0.2}$Se$_2$ films[2] and Co$_{40}$Fe$_{40}$B$_{10}$Dy$_{10}$ films[12] decreases as thickness increases. The optical properties also demonstrate strong thickness dependence. For instance, the band gap of CuIn$_{0.8}$Ga$_{0.2}$Se$_2$ films,[2] polycrystalline CuO,[13] and ZnO films[10]

typically narrows as thickness increases, while the ultraviolet photoluminescence of ZnO films strengthens.[14] The size effect extends to thermal properties as well; for example, the thermal conductivity of materials such as graphene and polycrystalline Pt nanofilms can be effectively modulated by their lateral dimensions and thickness.[15–17]

However, the size effect is not significant in all cases. Some properties, such as the thermal stress and thermal expansion coefficient of Cu films[18] and the transparency of ZnO films,[14] appear almost thickness-insensitive. These exceptions highlight the complexity of size-dependent behaviors and motivate comprehensive theoretical and experimental investigations to understand the intricate relationship between thickness and material properties.

Among various thin-film systems, perovskite materials stand out due to their flexible ABX$_3$-type crystal structure, with a wide range of choices for A- and B-site cations as well as X-site anions. This compositional freedom enables extensive tunability of electrical, optical, and thermal properties.[19–23] While three-dimensional perovskite oxides have been extensively studied, the effects of thickness on the electronic and optical properties of 2D perovskite oxide films remain underexplored.

In this study, we investigate how thickness governs the electronic structures and optical properties of two typical 2D perovskite films, namely 2D CdTiO$_3$ (CTO) and SrTiO$_3$ (STO) films, by using first-principles calculations. STO, often referred to as a "fruit fly" in solid state physics, has enabled numerous

[a]School of Civil Engineering, Wuhan University, Hubei, 430072, China

[b]Henan International Joint Laboratory of Nanocomposite Sensing Materials, Anyang Institute of Technology, Anyang, 455000, China. E-mail: 20180015@ayit.edu.cn

[c]Baoshun (Henan) New Carbon Material Co., Ltd, Anyang, 455000, China

foundational discoveries and was the first perovskite oxide whose freestanding film was realized at a single unit-cell limit.[24] In contrast, CTO is noteworthy due to its potential novel electronic properties stemming from unique conduction bands that are largely formed by the Cd 5s orbital.[25,26] This work compares the thickness-dependent modulation of the electronic structures and optical properties in these two systems and explores the underlying mechanisms in order to answer several important scientific questions, such as "How do the differences in orbital characteristics at the CBM between 2D STO and CTO films lead to thickness-dependent behaviors?" "Is the spatial distribution of electronic states at the VBM and CBM different between these two films, and what impact does this difference have on their optical properties?" and "How do their surface electronic properties change with thickness, and what are the reasons?" The study of these issues not only deepens our understanding of the structure–property relationship in 2D perovskite films, but also provides a crucial theoretical foundation for the rational design and optimization of related materials, particularly complex heterojunctions.

2. Computational methodology

2.1 Density functional theory calculation details

All first-principles calculations were performed using the projector augmented plane-wave (PAW) method,[27,28] as implemented in the Vienna *ab initio* simulation package (VASP).[29,30] The exchange–correlation interactions were treated within the framework of the generalized gradient approximation (GGA) using the Perdew–Burke–Ernzerhof (PBE) functional.[31] A plane-wave energy cutoff of 450 eV was employed throughout all calculations. The electronic self-consistency and ionic relaxation loops were converged to an energy threshold of 10^{-5} eV and a force threshold of 0.02 eV $\times$ Å^{-1}, respectively.

To minimize spurious interactions between periodic images in the out-of-plane direction, a vacuum layer exceeding 15 Å was introduced. Additionally, dipole correction was applied to improve convergence behavior.[32] The Brillouin zone sampling was performed using a $4 \times 4 \times 1$ and $10 \times 10 \times 1$ Monkhorst–Pack[33] k-grid for structural relaxation and static calculation, respectively. The 2D (001)-oriented CTO and STO films, with thickness ranging from 1 to 6 unit cells (u.c.), were simulated. For the convenience of discussion, these films are denoted as $n$uc-STO and $n$uc-CTO, respectively, where n stands for the film thickness.

2.2 Electronic properties

The carrier effective mass (m^*) is a vital descriptor for evaluating electronic transport properties in devices like photovoltaics, transistors, and thermoelectrics. It is fundamentally understood as the inverse of band curvature near the band edges. The effective mass is defined in terms of the second derivative of the band energy (E) with respect to the wave vector (k):[34]

$$m^* = \hbar^2 \left(\frac{\partial^2 E}{\partial^2 k}\right)^{-1} \tag{1}$$

where $\partial^2 E / \partial^2 k$ describes the energy band curvature. A steeper band corresponds to a higher curvature and thus smaller effective mass, which correlates with faster carrier dynamics and better mobility. In this study, the effective masses of electrons and holes in 2D CTO and STO films with varying thicknesses were calculated by using VASPkit software.[35]

To comprehensively analyze surface electronic behaviors, we investigated the work function of the thin films across different thicknesses *via* the planar averaged potential (PAP) method. The work function, which is the minimum energy required for an electron to escape the surface, provides a direct insight into the surface electron affinity and chemical reactivity of materials. This makes the work function a critical parameter for understanding charge transfer at heterointerfaces and for tuning catalytic properties in surface reactions.

2.3 Optical properties

We also analyzed the optical properties by computing the squared transition dipole moment (P^2) between the valence band maximum (VBM) and the conduction band minimum (CBM) using VASPkit software. This parameter is a quantitative measure of the optical transition probability, which directly governs the efficiency of light absorption and emission in optoelectronic applications.[36,37]

3. Results and discussion

3.1 Effect of film thickness on electronic structures

The 2D CTO and STO films exhibit indirect band gap characteristics, similar to their bulk counterparts, as shown in Fig. 1 and S1–S2. In both cases, the VBM is located at the M point of the Brillouin zone, while the CBM is at the G point. In addition, the partial density of states (PDOS) plots in Fig. 2 and S3 indicate that the electronic states at the VBM in both 2D CTO and STO films originate primarily from the O-2p orbitals. However, the orbital character at the CBM differs between the two systems: electronic states are primarily contributed by Cd-5s orbitals in 2D CTO films, whereas those of 2D STO films are contributed by Ti-3d orbitals.

The influence of film thickness on band gaps can be seen from Fig. 1 and S1–S2, where the band gap of both 2D CTO and STO films gradually decreases as the film thickness increases. Specifically, the band gap of the 2D CTO films decreases from 1.155 eV at a single unit-cell thickness to 0.097 eV at six unit-cell thickness. Similarly, the band gap of the 2D STO films decreases from 1.787 eV to 0.632 eV across the same thickness range. Furthermore, the valence band degeneracy of 2D CTO films at the VBM increases with thickness; in other words, more valence bands converge at point M, whereas their conduction bands remain non-degenerate at the CBM, *i.e.* containing only one energy band at the CBM. This non-degenerate character arises from the highly dispersive Cd-5s-orbital derived conduction bands, which results in higher carrier mobility at the CBM than the less-dispersive Ti-3d-orbital derived conduction bands in STO films.[25] The increased degeneracy at the VBM in thicker 2D CTO films introduces additional scattering channels, thereby
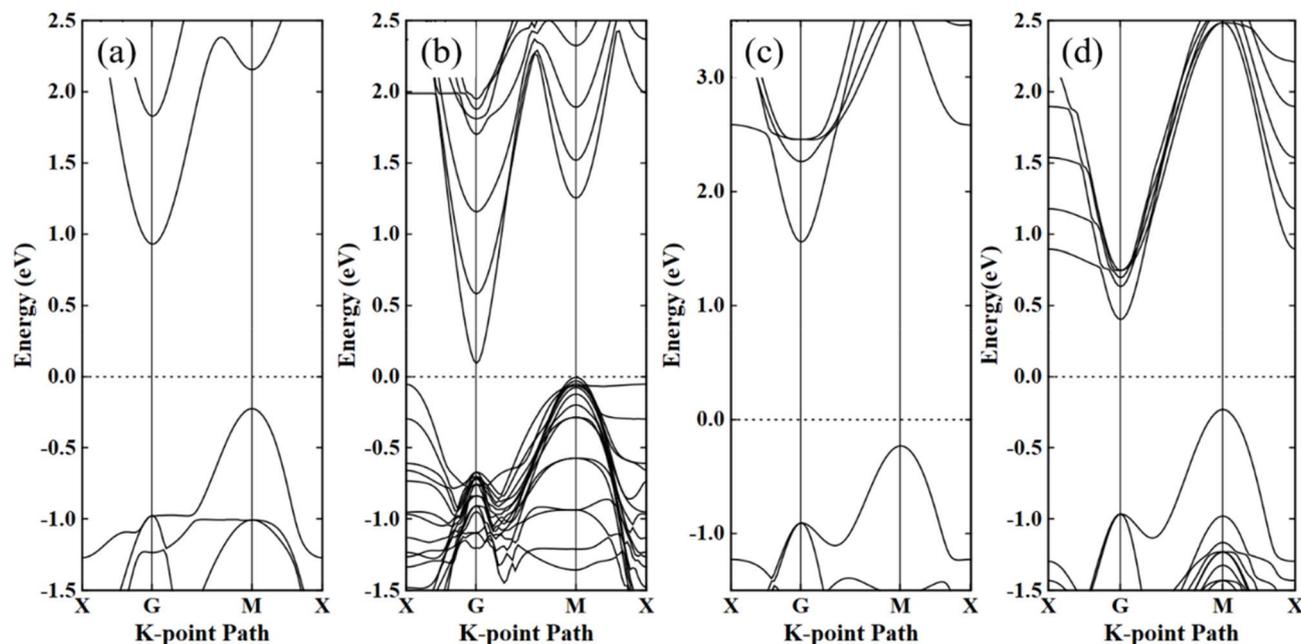
Fig. 1 Energy bands of 2D CTO and STO films with different thicknesses: (a) 1uc-CTO, (b) 6uc-CTO, (c) 1uc-STO, and (d) 6uc-STO. The Fermi level is set to zero and marked with a horizontal dashed line.

increasing the probability of carrier scattering. Conversely, 2D STO films remain non-degenerate at the VBM across all thicknesses. Consequently, thicker 2D CTO films have lower electronic scattering at the CBM, whereas 2D STO films exhibit comparatively lower hole scattering at the VBM.

The calculated carrier effective masses of 2D CTO and STO films at different thicknesses are shown in Table 1. The results indicate that the anisotropy of the effective mass is not significant in these two films, that is, the numerical changes in different directions of the reciprocal space are small, but the effective mass is greatly affected by film thickness. For 2D CTO films, the effective mass of holes at the VBM shows little

variation with thickness, remaining around 1.2 m_0. However, the effective mass of electrons at the CBM exhibits strong thickness dependence. Specifically, the electron effective mass is about 0.7 m_0 at a single-unit-cell thickness, deceasing to approximately 0.25 m_0 at six-unit-cell thickness. For 2D STO films, the hole effective mass at the VBM also exhibits weak thickness dependence, staying around 1.1 m_0. Different from 2D CTO films, the electron effective mass at the CBM of the 2D STO films remains nearly constant, with a value of about 0.4 m_0 across the whole thickness range.

The stability of the hole effective mass at the VBM in both 2D CTO and STO films can be attributed to the fact that their VBM
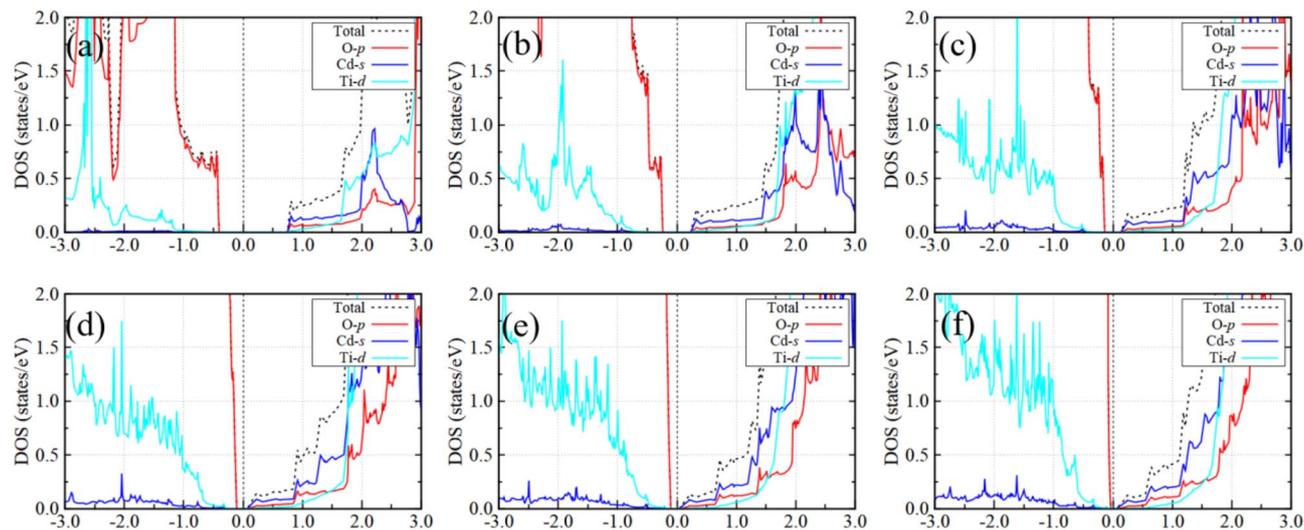

Fig. 2 Element-resolved DOS of 2D CTO films with different thicknesses: (a) 1uc-CTO, (b) 2uc-CTO, (c) 3uc-CTO, (d) 4uc-CTO, (e) 5uc-CTO, and (f) 6uc-CTO. The Fermi level (E_f) was set to zero and is indicated by a vertical dashed line in the above and each subsequent DOS diagram.

Table 1 Effective charge mass (in unit of m_0) of a hole (m_h^*) at the VBM and electron (m_e^*) at the CBM along a different k-path for 2D CTO films and 2D STO films with thickness from 1 u.c. to 6 u.c. Here, m_0 represents the mass of free electrons

	2D CTO films		2D STO films	
Thickness	m_h^*/m_0	m_e^*/m_0	m_h^*/m_0	m_e^*/m_0
1 u.c.	$(M \rightarrow G) = 1.300$	$(G \rightarrow M) = 0.718$	$(M \rightarrow G) = 1.085$	$(G \rightarrow M) = 0.421$
	$(M \rightarrow X) = 1.250$	$(G \rightarrow X) = 0.682$	$(M \rightarrow X) = 1.052$	$(G \rightarrow X) = 0.414$
2 u.c.	$(M \rightarrow G) = 1.237$	$(G \rightarrow M) = 0.477$	$(M \rightarrow G) = 1.089$	$(G \rightarrow M) = 0.446$
	$(M \rightarrow X) = 1.191$	$(G \rightarrow X) = 0.448$	$(M \rightarrow X) = 1.062$	$(G \rightarrow X) = 0.436$
3 u.c.	$(M \rightarrow G) = 1.211$	$(G \rightarrow M) = 0.369$	$(M \rightarrow G) = 1.099$	$(G \rightarrow M) = 0.452$
	$(M \rightarrow X) = 1.163$	$(G \rightarrow X) = 0.348$	$(M \rightarrow X) = 1.069$	$(G \rightarrow X) = 0.442$
4 u.c.	$(M \rightarrow G) = 1.170$	$(G \rightarrow M) = 0.306$	$(M \rightarrow G) = 1.112$	$(G \rightarrow M) = 0.457$
	$(M \rightarrow X) = 1.119$	$(G \rightarrow X) = 0.293$	$(M \rightarrow X) = 1.079$	$(G \rightarrow X) = 0.448$
5 u.c.	$(M \rightarrow G) = 1.161$	$(G \rightarrow M) = 0.271$	$(M \rightarrow G) = 1.104$	$(G \rightarrow M) = 0.465$
	$(M \rightarrow X) = 1.132$	$(G \rightarrow X) = 0.263$	$(M \rightarrow X) = 1.089$	$(G \rightarrow X) = 0.455$
6 u.c.	$(M \rightarrow G) = 1.137$	$(G \rightarrow M) = 0.252$	$(M \rightarrow G) = 1.114$	$(G \rightarrow M) = 0.460$
	$(M \rightarrow X) = 1.111$	$(G \rightarrow X) = 0.246$	$(M \rightarrow X) = 1.082$	$(G \rightarrow X) = 0.450$

states are primarily derived from O-2p orbitals, and in both systems the O atoms form Ti–O octahedra, which create similar local chemical environments for O atoms, resulting in similar band curvatures and thus weak thickness dependence of the hole effective mass. In contrast, the distinct electron effective mass at the CBM arises from different orbital origins: in 2D CTO films the CBM is dominated by Cd-5s states, whereas in 2D STO films it is governed by Ti-3d states.

As shown in Fig. 3(a), (b) and S4, within the thickness range studied here, although the two surfaces of the 2D CTO films consist of different atomic layers (one end being a TiO layer and the other a CdO layer), the potential difference between these two surfaces is very small, which indicates that the electron affinity on these two surfaces is similar. It is worth mentioning that this phenomenon differs significantly from the situation in 2D STO films, as illustrated in Fig. 3(c), (d) and S5, and other 2D perovskite films we have previously studied, such as 2D PbTiO$_3$ and BaTiO$_3$ films.[26] In these systems, there is a significant potential difference between the upper and lower surfaces (the

planar average potential on the AO layer is higher than that on the BO layer, where A = Sr, Ba, Pb, and B = Ti), indicating distinct electron affinity between the upper and lower surfaces.

In order to provide quantitative information for the uniqueness of the electron affinity on the surfaces of CTO films, this study also calculated the difference between the work function of the upper and lower surfaces of CTO films and STO films under different thickness, and the results are shown in Fig. S6. It can be seen from Fig. S6 that the work function difference between the upper and lower surfaces of STO films is large (above 2 eV), which is similar to the results previously obtained in other perovskite films, such as PbTiO$_3$ films and BaTiO$_3$ films, while the work function difference between the upper and lower surfaces of CTO films is small (within 0.3 eV).

3.2 Effect of film thickness on optical properties

To quantitatively assess the optical transition probability between the VBM and CBM, P^2 was calculated, as shown in
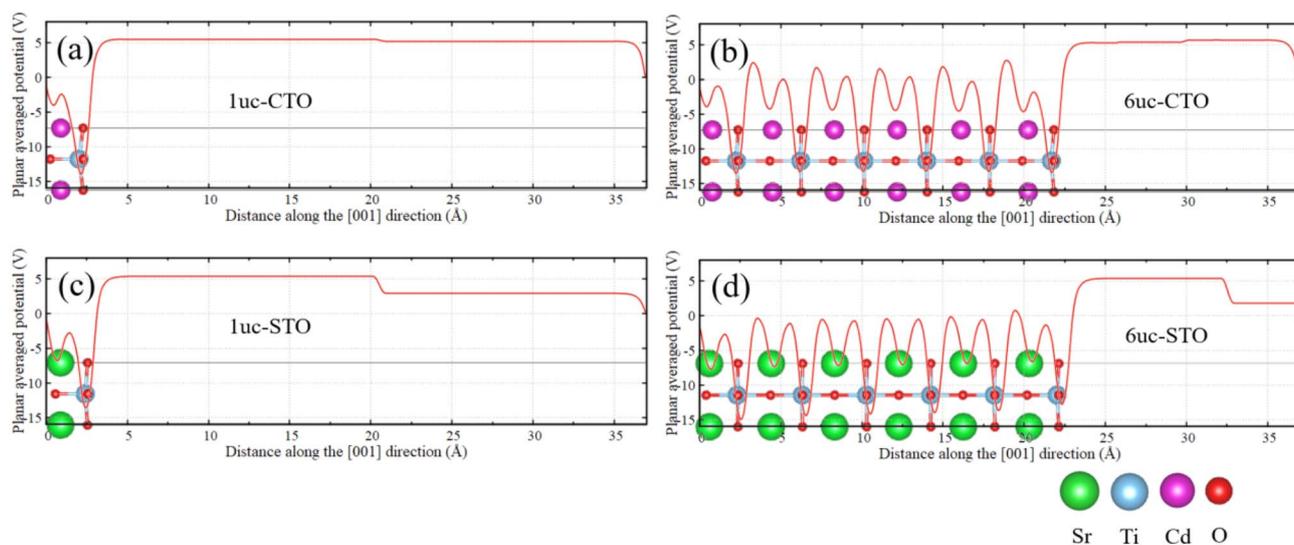

Fig. 3 The planar averaged potential (PAP) of 2D CTO and STO films with different thicknesses: (a) 1uc-CTO, (b) 6uc-CTO, (c) 1uc-STO, and (d) 6uc-STO. The corresponding atomic structures are also given in the pictures and aligned to the PAP curves.
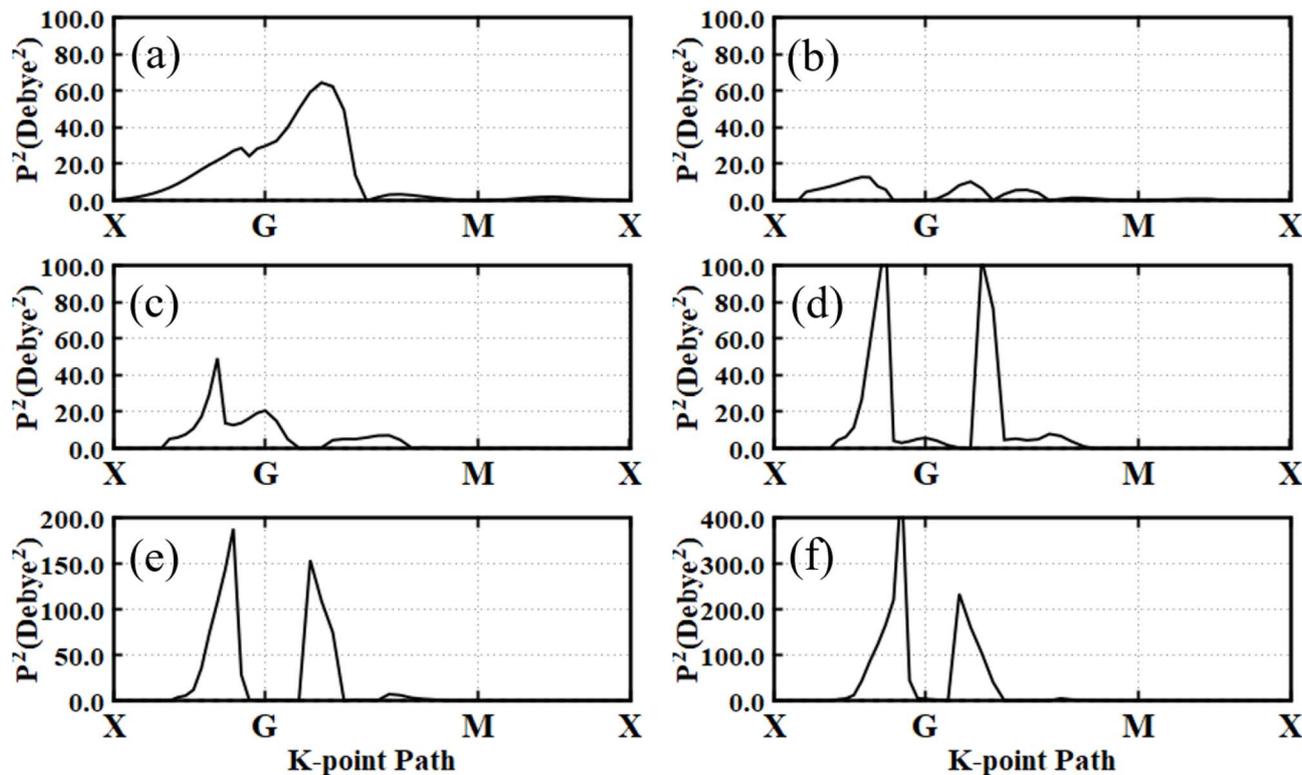
Fig. 4 The squares (in units of Debey^2) of the transition dipole moment of 2D CTO films with different thicknesses: (a) 1uc-CTO, (b) 2uc-CTO, (c) 3uc-CTO, (d) 4uc-CTO, (e) 5uc-CTO, and (f) 6uc-CTO.

Fig. 4 and 5. In 2D CTO films, the transition probability is relatively low when the film thickness is within three-unit cell. However, as the thickness increases beyond this threshold, the transition probability increases significantly, indicating enhanced optical activity in thicker CTO films. Moreover, it is worth mentioning that, in thicker 2D CTO films, the peak of the transition probability does not occur at the high-symmetry G or M points, but at the intermediate k-points in the Brillouin zone.

In contrast, 2D STO films exhibit the highest transition probability at a single-unit-cell thickness, with the peak located at the G point, as shown in Fig. 5. When the thickness reaches or exceeds two unit-cell layers, the transition probability drops sharply, becoming nearly negligible. This highlights a strong suppression of optical transitions in thicker STO films, in stark contrast to the trend observed in CTO films. These results highlight that ultrathin STO films and thicker CTO films may be more favorable for optoelectronic applications involving light absorption or emission.

The strength of the transition dipole moment is closely related to the spatial overlap between the ground and excited electronic states, that is, the greater the overlap, the stronger the transition dipole moment. To analyze the causes of the differences in transition probability mentioned above, this study calculated the electronic state distributions of 2D CTO and STO films at the VBM and CBM, and the results are shown in Fig. 6 and S7.

In 2D CTO films, the electronic states at the CBM are distributed on the Cd atoms of multiple (001) CdO layers, while the electronic states at the VBM are mainly distributed on the O atoms of the surface TiO layer and near-surface TiO layers. The distance between the VBM states and CBM states is short, which promotes the overlap of electronic states, enhances their mutual interaction and thus improves the transition probability.

In contrast, the CBM states of STO films are highly localized on the Ti atoms of the surface TiO layer, while the electronic states at the VBM are localized on the O atoms of the TiO layer immediately under the SrO surface. At a single unit cell thickness, the spatial proximity between the VBM and CBM states is the shortest (Fig. S7), resulting in the highest electron transition probability. However, as the film thickness increases, the spatial separation of these two states widens, weakening the interaction between them. This significantly reduces the transition probability, thereby suppressing the optical activity in thicker STO films.

The reason for the aforementioned phenomena may be attributed to the different orbital characteristics at the CBM in 2D CTO and STO films. Due to the spherical symmetry of the 5s orbital, the Cd 5s orbitals in different CdO layers can interact with each other, and they can be combined together to form delocalized orbitals. In contrast, the Ti $3d_{xy}$ orbital extends along the (001) TiO layer, preventing overlap between Ti $3d_{xy}$ orbitals that are on different (001) TiO layers. Consequently, the electronic states at the CBM that are derived from the Ti $3d_{xy}$ orbitals exhibit strong localization. This localization inhibits interlayer electronic interaction and suppresses optical transition probabilities, particularly in thicker STO films.
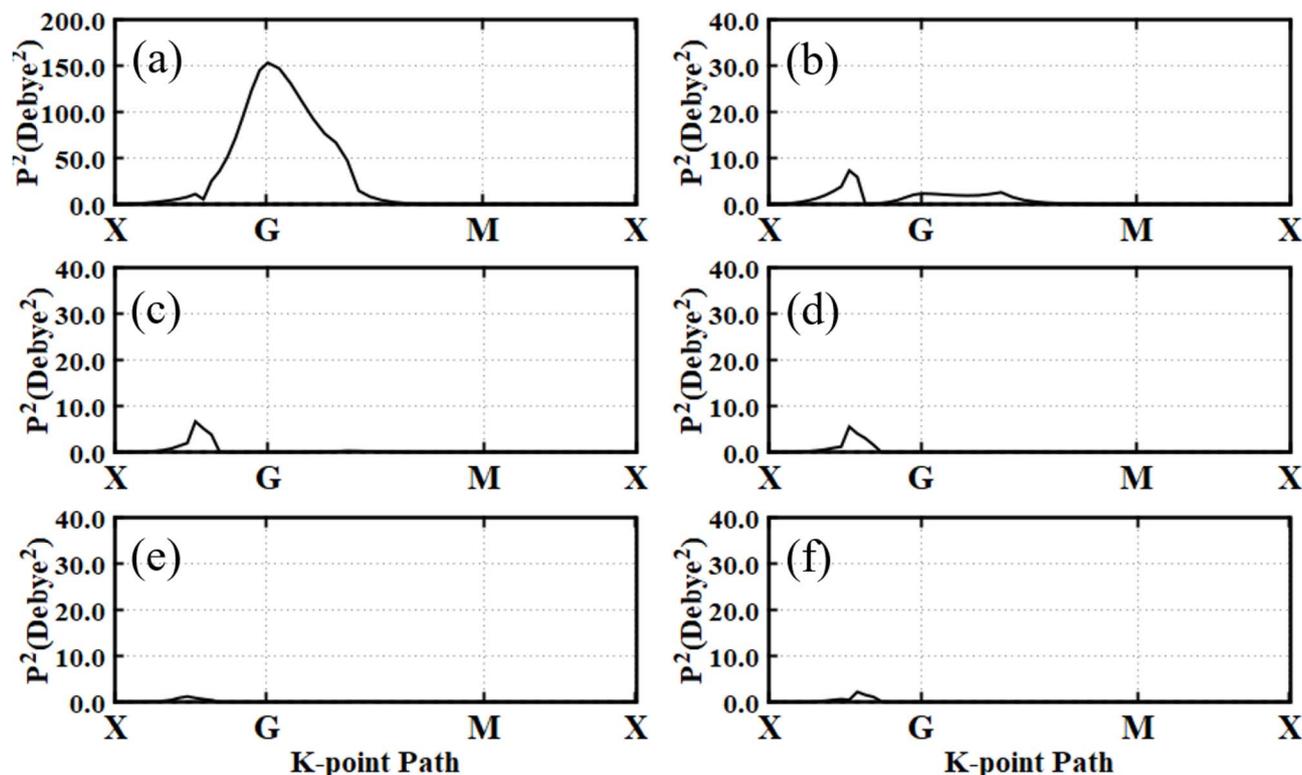
Fig. 5 The squares (in units of Debey^2) of the transition dipole moment of 2D STO films with different thicknesses: (a) 1uc-STO, (b) 2uc-STO, (c) 3uc-STO, (d) 4uc-STO, (e) 5uc-STO, and (f) 6uc-STO.
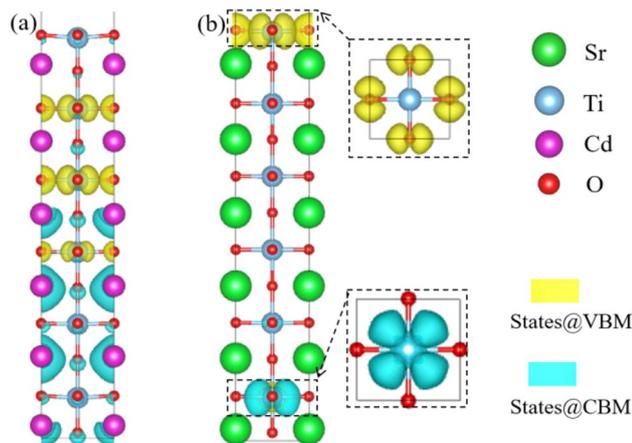

Fig. 6 Side views of the electronic state distributions, projected at the VBM and CBM for (a) 6uc-CTO and (b) 6uc-STO. In panel (b), the top views of the electronic state distributions on the topmost and down-most (001) TiO-layers are also presented.

Last but not least, we would like to have some discussions on the accuracy of our calculations. It is well-established that the standard GGA/PBE approach may lead to an inaccurate description of electronic properties of the systems containing 3d or 4f electrons. We have considered the exchange correlation effect among Ti 3d electrons at the level of +U correction. The band structures and PDOS of CTO and STO films with and without +U correction are shown in Fig. S8 and S9. In the

calculation, the effective Hubbard parameter (U_{eff}) was set at 5.6 eV for Ti 3d orbitals, which was determined by a linear response approach proposed by Cococcioni *et al.*[38] From these figures, it can be seen that after +U correction, except for an increase in the band gap of STO films, there is basically no significant change in the key electronic structures, *i.e.* the band structures and PDOS of CTO and STO films. After +U correction, the orbital composition of both CTO and STO films at the VBM and CBM did not change, and the trend of band gap with thickness in both systems remained unchanged, too. So, we believe that performing +U correction will not have a substantial impact on the existing conclusions.

4. Conclusions

This study systematically investigates the influence of film thickness ranging from 1 u.c. to 6 u.c., on the electronic and optical properties of 2D CTO and STO films using first-principles calculations. Both of these films exhibit an indirect band gap, with band gap values decreasing monotonically as thickness increases. Specifically, the band gap of 2D CTO films reduces from 1.155 eV (1 u.c. thick) to 0.097 eV (6 u.c. thick), while that of STO films decreases from 1.787 eV to 0.632 eV over the same thickness range. Furthermore, the electron effective mass in 2D CTO films shows a pronounced reduction from 0.7 m_0 to 0.25 m_0 with increasing thickness, whereas it remains relatively stable at around 0.4 m_0 in STO films. Additionally, the hole effective masses in both of these 2D films exhibit minimal

dependence on thickness, remaining nearly unchanged throughout the thickness range studied.

For optical properties, 2D CTO films show a significant enhancement in transition probability once the thickness exceeds three unit-cell layers. In contrast, 2D STO films exhibit the maximum transition probability at a thickness of one unit cell, which then rapidly diminishes to near zero with further increment in thickness. These differences can be attributed to the difference in the spatial distribution of electronic states at the VBM and CBM in these two materials. Overall, the results demonstrate that the electronic and optical properties of 2D CTO films are more strongly modulated by thickness than those of 2D STO films, which makes 2D CTO films a more promising candidate for thickness-engineered optoelectronic applications.

Author contributions

H. H.: conceptualization, data curation, formal analysis, investigation, methodology, writing – original draft. Y. X.: conceptualization, project administration, supervision, writing – review & editing. C. H.: data curation, writing – review & editing. X. B.: methodology, writing – review & editing.

Conflicts of interest

There are no conflicts to declare.

Data availability

The data supporting this article have been included as part of the supplementary information (SI). Supplementary information: energy bands of 2D CTO and STO films with different thickness; element-resolved DOS of 2D CTO and STO films with U correction; planar averaged potential of 2D CTO and STO films; work function difference between the upper and lower surfaces as a function of film thickness; electronic state distributions projected at VBM and CBM. See DOI: https://doi.org/10.1039/d5na01018g.

Acknowledgements

References

1 P. Yang, L. Li, S. Yu, H. Zheng and W. Peng, *Appl. Surf. Sci.*, 2019, **493**, 396–403.
2 P. K. Mishra, Y. K. Gautam, A. Kumar, R. K. Jain, J. N. Prasad, A. K. Choudhary and R. Chandra, *AIP Conf. Proc.*, 2014, **1576**, 33–37.
3 Y. Xue, Y. Guo and C. Geng, *Appl. Surf. Sci.*, 2021, **563**, 150268.
4 T. M. Mukametkali, X. S. Rozhkova, A. K. Aimukhanov, B. R. Ilyassov, K. Apshe, A. K. Zeinidenov and B. U. Karaganda, *Phys. Ser.*, 2023, **111**(3), 107–118.
5 L. Najafi, B. Taheri, B. Martin-Garcia, S. Bellani, D. Di Girolamo, A. Agresti, R. Oropesa-Nunez, S. Pescetelli, L. Vesce, E. Calabro, M. Prato, A. E. Del Rio Castillo, A. Di Carlo and F. Bonaccorso, *ACS Nano*, 2018, **12**(11), 10736–10754.
6 D. Bera, L. Qian, T.-K. Tseng and P. H. Holloway, *Materials*, 2010, **3**(4), 2260–2345.
7 B. Das, I. Aguilera, U. Rau and T. Kirchartz, *Adv. Opt. Mater.*, 2022, **10**(13), 2101947.
8 H. S. Das, S. Maity, S. Bhattacharyya, A. Bag, G. Roymahapatra, S. Banerjee, H. Maity, A. Pereira and B. Bepari, *ES Gen.*, 2024, **6**, 1292.
9 S.-P. Yoon, S.-J. Park, A. Park, J. Byun, B. Park and M.-J. Lee, *Korean J. Chem. Eng.*, 2024, **41**(14), 3783–3789.
10 H. I. Efkere, A. Tataroglu, S. S. Cetin, N. Topaloglu, M. P. Gonullu and H. Ates, *J. Mol. Struct.*, 2018, **1165**, 376–380.
11 S. Sarkar, S. Kumar, P. Raychaudhuri and P. Ayyub, *AIP Conf. Proc.*, 2013, **1536**, 253–254.
12 W.-J. Liu, Y.-H. Chang, C.-C. Chiang, Y.-T. Chen, Y.-Z. Wang, C.-L. Wu, S.-H. Lin and S.-L. Ou, *Materials*, 2023, **16**(17), 5995.
13 B. D. Aparicio-Huacarpuma, C. A. Vilca-Huayhua, A. P. Silveira, S. N. Báo, S. W. da Silva and J. A. H. Coaquira, *J. Alloys Compd.*, 2025, **1014**, 178681.
14 R. Pérez-Cuapio, M. Pacio, H. Juarez, J. A. Alvarado, C. Guarneros, C. Bueno and A. Pacio, *J. Nano. Res.*, 2018, **52**, 102–114.
15 S. Yang, P. He, H. Zheng, D. Xiao and G. Ding, *Chem. Eng. J.*, 2024, **493**, 152803.
16 Q. G. Zhang, B. Y. Cao, X. Zhang, M. Fujii and K. Takahashi, *J. Phys. Condens. Matter*, 2006, **18**(34), 7937–7950.
17 S. Edalatpour and M. Francoeur, *J. Quant. Spectrosc. Radiat. Transfer*, 2013, **118**, 75–85.
18 S. Hwang and Y. Kim, *J. Nanosci. Nanotechnol.*, 2011, **11**(2), 1555–1558.
19 M. Yang, D. H. Kim, T. R. Klein, Z. Li, M. O. Reese, B. J. Tremolet de Villers, J. J. Berry, M. F. A. M. van Hest and K. Zhu, *ACS Energy Lett.*, 2018, **3**(2), 322–328.
20 Z. Zhang, Z. Li, L. Meng, S. Y. Lien and P. Gao, *Adv. Funct. Mater.*, 2020, **30**(38), 2001904.
21 H.-S. Kim and N.-G. Park, *Appl. Phys. Rev.*, 2025, **12**(2), 021313.
22 L. Li, Y. Hu, Y. Chen, C. Wang, G. Zhao, X. Du, C. Wang, L. Xiao, Z. Lu, J. Wang, D. Wang, J. Jie, J. Huang and G. Zou, *Adv. Funct. Mater.*, 2023, **33**(29), 2301205.
23 C. Fang, H. Wang and D. Li, *2D Materials*, 2021, **8**(2), 022006.
24 D. Ji, S. Cai, T. R. Paudel, H. Sun, C. Zhang, L. Han, Y. Wei, Y. Zang, M. Gu, Y. Zhang, W. Gao, H. Huyan, W. Guo, D. Wu, Z. Gu, E. Y. Tsymbal, P. Wang, Y. Nie and X. Pan, *Nature*, 2019, **570**(7759), 87–90.
25 L. Fang, C. Chen, A. Sundaresan, C. Narayana, N. Ter-Oganessian, A. P. Pyatakov, S. Cao, J. Zhang and W. Ren, *Nanoscale*, 2021, **13**(18), 8506–8513.

26 Y. Xue, X. Bai, Y. Guo and C. Geng, *Surf. Interfaces*, 2024, **45**, 103929.

27 P. E. Blöchl, *Phys. Rev. B: Condens. Matter Mater. Phys.*, 1994, **50**(24), 17953–17979.

28 G. Kresse and D. Joubert, *Phys. Rev. B: Condens. Matter Mater. Phys.*, 1999, **59**(3), 1758–1775.

29 G. Kresse and J. Furthmuller, *Comput. Mater. Sci.*, 1996, **6**, 15–50.

30 G. Kresse and J. Furthmüller, *Phys. Rev. B: Condens. Matter Mater. Phys.*, 1996, **54**(16), 11169–11186.

31 J. P. Perdew, K. Burke and M. Ernzerhof, *Phys. Rev. Lett.*, 1996, **77**, 3865–3868.

32 L. Bengtsson, *Phys. Rev. B: Condens. Matter Mater. Phys.*, 1999, **59**(19), 12301–12304.

33 H. J. Monkhorst and J. D. Pack, *Phys. Rev. B: Condens. Matter Mater. Phys.*, 1976, **13**(12), 5188–5192.

34 L. D. Whalley, J. M. Frost, B. J. Morgan and A. Walsh, *Phys. Rev. B*, 2019, **99**(8), 085207.

35 V. Wang, N. Xu, J.-C. Liu, G. Tang and W.-T. Geng, *Comput. Phys. Commun.*, 2021, **267**, 108033.

36 W. Meng, X. Wang, Z. Xiao, J. Wang, D. B. Mitzi and Y. Yan, *J. Phys. Chem. Lett.*, 2017, **8**(13), 2999–3007.

37 J. Luo, X. Wang, S. Li, J. Liu, Y. Guo, G. Niu, L. Yao, Y. Fu, L. Gao, Q. Dong, C. Zhao, M. Leng, F. Ma, W. Liang, L. Wang, S. Jin, J. Han, L. Zhang, J. Etheridge, J. Wang, Y. Yan, E. H. Sargent and J. Tang, *Nature*, 2018, **563**(7732), 541–545.

38 M. Cococcioni and S. de Gironcoli, *Phys. Rev. B: Condens. Matter Mater. Phys.*, 2005, **72**, 035105.